Research Article

Impact of baffle on forced convection heat transfer of CuO/water nanofluid in a micro-scale backward facing step channel

Shailendra RANA[1],* , Hari Bahadur DURA[1] , Sudip BHATTRAI[1] , Rajendra SHRESTHA[1]

[1]*Department of Mechanical and Aerospace Engineering, Pulchowk Campus, Institute of Engineering, Tribhuvan University, Kathmandu, Nepal*

ARTICLE INFO

ABSTRACT

Numerical simulations have been carried out to investigate the thermal-hydraulic characteristics using water-based CuO nanofluid with volume fraction (ϕ) = 0 – 5% and fixed nanoparticle size (d_p) = 20 nm at Reynolds numbers (Re) = 100 – 389 in a micro-scale backward facing step channel with and without a baffle using finite volume method. The flow is steady, laminar, and incompressible. The channel has an expansion ratio (ER) = 1.9423 with a fixed step height (S) of 490 μm. To study the effect of the baffle, different geometrical configurations have been developed by varying its height and location. The height of the baffle is varied as H_b = 160 – 640 μm. The baffle is stationed on the upper wall of the channel at a dimensionless distance (D) = 1, 2, 3 and 4. The upstream, step and upper walls are thermally insulated while the lower wall downstream of the step is under a constant heat flux (q_s'') = 20000 W/m². The parameters of interest for analysis are Nusselt number, skin friction coefficient and velocity distribution under different flow conditions. Results indicate that the rise in volume fraction and Reynolds number enhances the Nusselt number, indicating improved heat transfer. However, the skin friction coefficient decreases with the increment in Reynolds number. The increase in baffle height causes the Nusselt number and skin friction coefficient to rise. As the baffle is moved away from the step, the Nusselt number tends to decrease. In comparison to water, the heat transfer improved by about 164% using CuO nanofluid at Re = 389 with ϕ = 5% in the presence of the baffle with H_b = 640 μm and D = 1. However, the heat transfer enhancement has been achieved at the cost of higher pumping power requirements.

Cite this article as: Shailendra R, Hari B D, Sudip B, Rajendra S. Impact of baffle on forced convection heat transfer of CuO/water nanofluid in a micro-scale backward facing step channel. J Ther Eng 2022;8(3):310–322.

*Corresponding author.
*E-mail address: ranashailendra74@gmail.com

INTRODUCTION

Sudden expansion occurs in many engineering applications such as microelectronics, gas turbines, combustion chambers, heat exchangers, etc. [1]. The prominent features of sudden expansion problems are the occurrence of flow separation and subsequent reattachment. Channels with a backward facing step (BFS) configuration are one of the widely investigated topics in fluid mechanics. In such geometries, the occurrence of flow separation leads to generation of turbulence in the recirculation zone which enhances mixing between fluids, and consequently improves heat transfer.

Over the years, heat transfer augmentation has been achieved by implementing several active and passive techniques such as geometry modifications, use of ribs and baffles, use of nanoparticles, etc. Among these techniques, nanofluids are considered to be one of the effective methods of enhancing the thermal performance of engineering systems. The prominent characteristic of such fluids is their enhanced thermophysical properties which facilitate heat transfer. The preparation of these fluids requires the suspension of nanoparticles into the conventional base fluids such as water, ethylene glycol, etc. [2].

In the past two decades, rapid progress has been made regarding heat transfer enhancement using nanofluids. Guo [3] provided a comprehensive review of the implementation of nanofluids for heat transfer enhancement. There have been massive numerical and experimental studies on heat transfer augmentation using nanofluids in different geometrical configurations with applications to different thermal systems. Abu-Nada et al. [4] numerically investigated the effect of nanofluids on heat transfer characteristics over a backward facing step using the finite volume method. Kherbeet et al. [5] utilized the finite volume method to study the mixed convection heat transfer over a microscale backward facing step under a constant heat flux condition using nanofluids with volume fractionsin the range of 1 – 4 % and nanoparticle size (d_p) = 25 – 70 nm. They found that SiO_2 nanofluid has the highest Nusselt number and Nusselt number increases with decreasing nanoparticle diameter. Ekiciler [6] performed a numerical investigation regarding laminar forced convection heat transfer utilizing Al_2O_3/water nanofluid in a duct having a single backward facing step configuration. He found that the Nusselt number increases with the rise in nanoparticle volume fraction and Reynolds number. Abdulvahitoglu [7] implemented an analytic hierarchy process to evaluate the performance of different nanofluids (Cu-water, NiO-water, and CuO-water) for engine cooling systems. He concluded that the Cu-water nanofluid is the most suitable coolant in terms of thermophysical properties as compared to the other nanofluids. Kilic et al. [8] numerically investigated the combined effect of the use of different working fluids(pure water, Al_2O_3/water, Cu/water, and TiO_2/water) and swirling jets on heat transfer in a rectangular channel of a vehicle radiator. They found that the average Nusselt number increased by 51.3% with the rise in Reynolds number from 12000 to 21000. The CuO/water nanofluid registered increments on the average Nusselt number by 3.6%, 7.6%, and 8.5% as compared to Ti/water, Al_2O_3/water, and pure water respectively.

Along with the utilization of nanofluids, researchers have also integrated the use of obstacles such as ribs, baffles, etc. to facilitate heat transfer in backward and forward facing steps. Heshmati et al. [9] numerically studied the forced convection heat transfer in a channel having backward facing steps with different expansion ratios in the presence of solid or slotted baffles at Re = 100 – 400. They concluded that the geometry with an expansion ratio of 2 and solid baffle has the highest Nusselt number compared to other geometries. They also found that a slotted baffle installed at the top wall instead of a solid baffle reduced the average Nusselt number. Alawi et al. [10] carried out a numerical study of laminar mixed convection flow using nanofluids (Al_2O_3, CuO, ZnO, SiO_2) with ϕ = 1 – 4 % and nanoparticle diameter in the range of 25 – 80 nm over a backward facing step with a vertical baffle under a constant heat flux condition in the range of 10 – 70 W/m². Their results indicated that the SiO_2 nanofluid has the highest Nusselt number in comparison to other nanofluids. The effects of baffle height, width, and distance on heat transfer characteristics are substantial.

The survey of existing literature suggests that no studies have been carried out to investigate the effects of a vertical baffle in a micro-scale backward facing step under a constant heat flux boundary condition utilizing CuO nanofluid. Hence, the current work aims to perform a thorough investigation of the effects of the vertical baffle on the laminar flow and heat transfer characteristics of water-based CuO nanofluid with ϕ = 0 – 5% and d_p = 20 nm at Re = 100 – 389. This work will further supplement our understanding of the flow and heat transfer characteristics of nanofluids in facing step channels. From design and application perspectives, our findings will be useful in the augmentation of heat transfer in thermal systems. Lastly, the results are presented in terms of Nusselt number, skin friction coefficient, and velocity contours for different Reynolds numbers and volume fractions.

PHYSICAL MODELING AND MATHEMATICAL FORMULATION

Physical Model

Two-dimensional laminar forced convection heat transfer of water-based CuO nanofluid in a micro-scale backward facing step (MBFS) channel in the presence of a thin solid baffle is numerically investigated. A baffle is installed on the upper wall of the channel at a dimensionless distance (D = d/H) away from the step. A diagrammatic representation of the physical model is shown in Figure 1. The MBFS channel
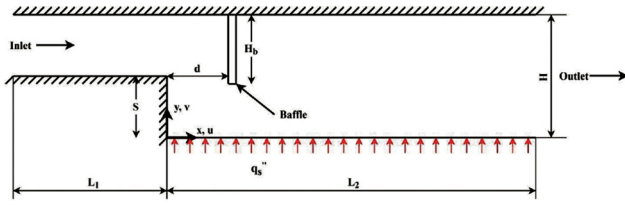
Figure 1. Computational model of micro-scale backward facing step channel with mounted baffle.

has an expansion ratio (ER = H/H-S) = 1.9423 with a fixed step height (S) of 490 μm. The inlet height of the channel is 520 μm. The upstream length (L_1) is $20 \times 10^3 \mu m$ whereas the downstream length (L_2) is $50 \times 10^3 \mu m$. The upstream, step and upper walls are thermally insulated whereas a constant heat flux (q_s'') = 20000 W/m² is applied at the downstream wall of the channel. The height and position of the baffle are varied to investigate their impacts on hydrodynamic and thermal characteristics in the channel. The baffle height is in the range of H_b = 160 – 640 μm whereas its position is varied by changing the distance (D) = 1, 2, 3 and 4. The flow at the channel inlet is steady and fully developed. The base fluid (water) and the CuO nanoparticles are in thermal equilibrium with each other and no-slip condition is considered. The flow is considered to be Newtonian and incompressible. Radiation heat transfer, viscous dissipation and internal heat generation are neglected in this study.

Governing Equations

Two-dimensional, steady, laminar and incompressible flow is considered. Accordingly, the continuity, momentum and energy equations can be expressed as [11]:

- Continuity equation:

$$\frac{\partial u}{\partial x} + \frac{\partial v}{\partial y} = 0 \qquad (1)$$

- Momentum equation:

$$u\frac{\partial u}{\partial x} + v\frac{\partial u}{\partial y} = -\frac{1}{\rho}\frac{\partial p}{\partial x} + \upsilon\left(\frac{\partial^2 u}{\partial x^2} + \frac{\partial^2 u}{\partial y^2}\right) \qquad (2)$$

$$u\frac{\partial v}{\partial x} + v\frac{\partial v}{\partial y} = -\frac{1}{\rho}\frac{\partial p}{\partial y} + \upsilon\left(\frac{\partial^2 v}{\partial x^2} + \frac{\partial^2 v}{\partial y^2}\right) \qquad (3)$$

- Energy equation:

$$u\frac{\partial T}{\partial x} + v\frac{\partial T}{\partial y} = -\frac{1}{\rho}\frac{\partial p}{\partial y} + \alpha\left(\frac{\partial^2 T}{\partial x^2} + \frac{\partial^2 T}{\partial y^2}\right) \qquad (4)$$

where υ represents the kinematic viscosity and α is the thermal diffusivity.

The Reynolds number has been expressed in terms of hydraulic diameter as follows:

$$\mathrm{Re} = \frac{\rho U\infty D_h}{\mu} \qquad (5)$$

where D_h is the hydraulic diameter equal to twice the channel inlet height and μ is the fluid viscosity.

Similarly, the Nusselt number (Nu) can be calculated as:

$$\mathrm{Nu} = \frac{hD_h}{k} \qquad (6)$$

where h is the heat transfer coefficient and k is the thermal conductivity of the working fluid.

The skin friction coefficient (C_f) can be computed as:

$$C_f = \frac{2\tau_W}{\rho U_\infty^2} \qquad (7)$$

where τ_w is the wall shear stress.

Thermophysical Properties of Nanofluids

The thermophysical properties of interest for CuO nanofluid are density, dynamic viscosity, specific heat capacity and thermal conductivity. The following theoretical relations have been utilized to approximate the effective properties of the CuO nanofluid:

The effective thermal conductivity can be calculated from the following relation [12]:

$$k_{static} = k_f\left(\frac{k_p + 2k_f - 2\phi(k_f - k_p)}{k_p + 2k_f + \phi(k_f - k_p)}\right) \qquad (8)$$

The effective viscosity has been determined from the empirical correlation provided by [13]:

$$\mu_{eff} = \frac{\mu_f}{1 - 34.87\left(\dfrac{d_p}{d_f}\right)^{-0.3}\phi^{1.03}} \qquad (9)$$

where μ_{eff} and μ_f are the viscosities of the nanofluid and the base fluid respectively. Similarly, ϕ is the nanoparticle volume fraction, d_p is the nanoparticle diameter and d_f is the diameter of the base fluid molecule.

The equivalent diameter of base fluid molecule (d_f) can be expressed as follows:

$$d_f = \left[\frac{6M}{N\pi\rho f_0}\right]^{1/3} \qquad (10)$$

where M is the molecular weight of the base fluid, N is the Avogadro number and subscripts f and p refer to the base

fluid and nanoparticle respectively. Here, ρ_{f_0} is the mass density of basefluid taken at reference temperature, $T_0 =$ 273 K.

The effective density of the nanofluid can be approximated by the following correlation as follows [13]:

$$\rho_{eff} = (1 - \phi)\rho_f + \phi\rho_p \tag{11}$$

where ρ_f and ρ_p are the densities of the basefluid and nanoparticles respectively.

The effective heat capacity of the nanofluid can be expressed as follows [14]:

$$(\rho C_p)_{eff} = (1 - \phi)(\rho C_p)_f + \phi(\rho C_p)_p \tag{12}$$

where $(\rho C_p)_f$ and $(\rho C_p)_{eff}$ are the heat capacities of the base fluid and the nanoparticles respectively. Table 1 provides the thermophysical properties of water and CuO at T = 300 K.

Grid Independence Study

To obtain a grid independent solution, nine progressively refined grids were generated using ICEM CFD software. The grid structure for the geometrical model without and with baffle is illustrated in Figures 2 (a-b). All the grids have expansion factors of 1.03 and 1.1 in the x- and y- directions respectively. The grid sizes range from 4×10^3 to 1.6×10^5 elements. Employing water as the working fluid, numerical simulations were carried out at Re = 100 for the

Table 1. Thermophysical properties of water and CuO at T = 300 K

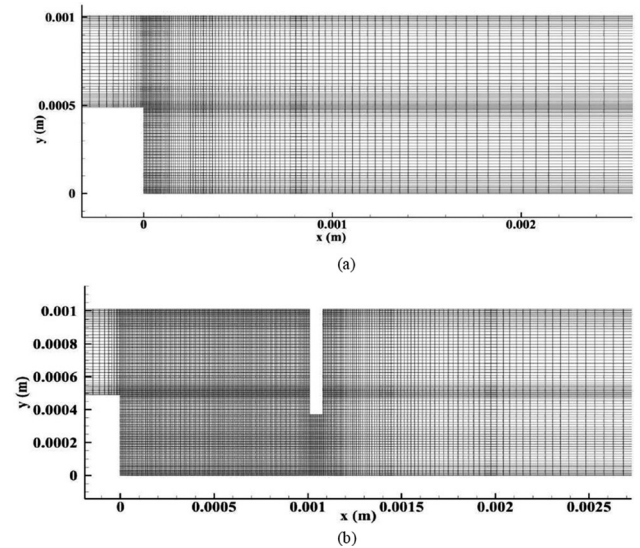| Particle type	ρ(kg/m³)	k(W/mK)	C_p(J/kgK)	μ(Pa.s)
Water	997.1	0.613	4179	0.001
CuO	6500	20	535.6	-

(a)

(b)

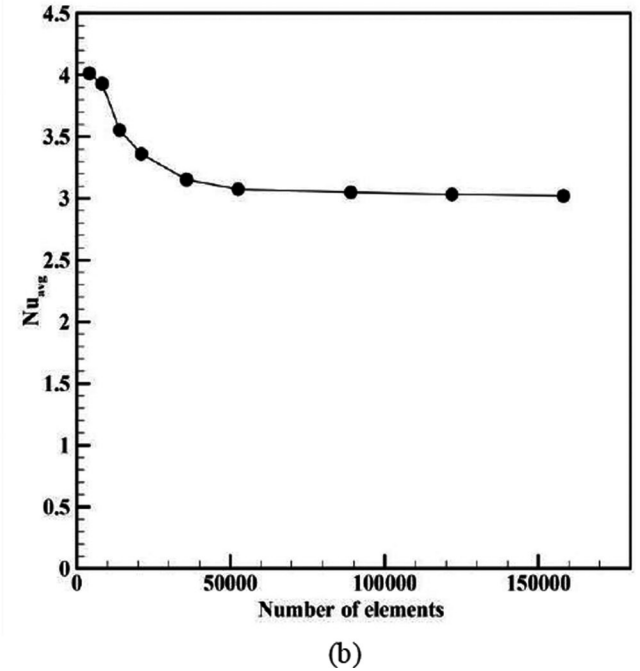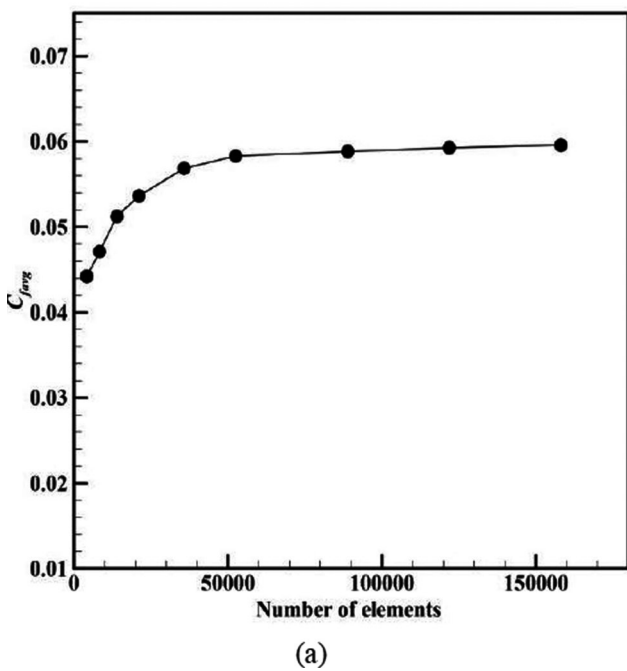**Figure 2.** Grid structure. (a) without baffle and (b) with baffle.

(a)

(b)

Figure 3. Grid independence study. (a) average Nusselt number and (b) average skin friction coefficient.

grid without baffle and the variation in the values of average Nusselt number and skin friction coefficient with increasing grid densities were obtained.

Figures 3(a-b) present the variation in the values of average Nusselt number and skin friction coefficient respectively. With the increase in the grid size from 5×10^4 to 1.6×10^5 elements, it is observed that the changes in the values of average Nusselt number and skin friction coefficient are 2.2% and 1.77% respectively. Consequently, the grid containing 5×10^4 elements has been selected in terms of solution accuracy and computational time.

Model Validation

The present numerical solutions have been validated against the experimental and numerical results of Armaly et al. [15]. The validation of the current model has been done in terms of the non-dimensionalised values of reattachment point and velocity distribution. In their study, they considered air as the working fluid. The present numerical solutions have been validated for Re = 100 and 389 using water as the working fluid. Table 2 presents the comparison of the reattachment lengths at Re = 100 and 389 against the published literature. Calculations show that the present results of the non-dimensionalised values of reattachment point at Re = 100 differ by 0.6711% against the experimental and numerical results of the published literature. Similarly, the present values of the non-dimensionalised reattachment point at Re = 389 showed differences of 2.06% and 3.2% against the experimental and numerical results respectively. Besides this, the comparison of non-dimensionalised profiles of velocity at Re = 100 and 389 at different stream-wise positions (x/S = 2.55 and 4.8) has also been done as shown in Figures 4 (a-d). Results indicate that the average deviations of x-velocity against the published literature at Re = 100 at x/S = 2.55 and 4.8 are 4.1% and 3.65% respectively. Similarly, the present results regarding the x-velocity at Re = 389 at x/S = 2.55 and 4.8 deviated by 2.38% and 2.25% respectively. Hence, our computational model demonstrates a good agreement with the published data.

Numerical Procedures

A finite volume method has been implemented in order to solve Equations (1)–(4) using commercially available ANSYS FLUENT software. The Semi-Implicit Method for Pressure-Linked Equations (SIMPLE) algorithm has been employed to couple the pressure and velocity fields. For spatial discretization, the second-order upwind scheme has been used for continuity, momentum and energy equations. The residual for solution convergence has been set to 10^{-8} for continuity, momentum and energy equations.

RESULTS AND DISCUSSION

This section deals with the impact of the vertical baffle on thermal-hydraulic characteristics using CuO nanofluid in the MBFS channel. The parameters of interest for analysis are Nusselt number, skin friction coefficient, and velocity distributions for different volume fractions and Reynolds numbers.

Effect of Volume Fraction
Nusselt number

The effect of volume fraction on Nusselt number has been studied at Re = 389 with ϕ = 0 – 5%. Figure 5 illustrates the distribution of local Nusselt number along the heated wall with increasing volume fraction. The results indicate that the heat transfer is augmented with the rise in volume fraction. This can be attributed to the fact that the thermal conductivity of the fluid is enhanced with increasing volume fraction. Due to the addition of nanoparticles, the rate of exchange of energy is enhanced due to their irregular and random motions in the fluid and thus contributes to more heat transfer [16].

Effect of Reynolds Number
Skin friction coefficient

The effect of Reynolds number on skin friction coefficient has been investigated at Re = 100 - 389 with ϕ = 5% and a fixed baffle height (H_b) = 640 μm installed at D = 1. Figure 6 (a) presents the distribution of local skin friction coefficient along the heated wall with increasing Reynolds numbers. It can be observed that the skin friction coefficient decreases with the rise in Reynolds number. The reason is that the skin friction coefficient is inversely proportional to Reynolds number.

Nusselt number

The distribution of Nusselt number with increasing Reynolds number has been studied. Figure 6 (b) shows the

Table 2: Comparison of the values of reattachment point against the experimental and theoreticaldata of Armaly et al. [15]

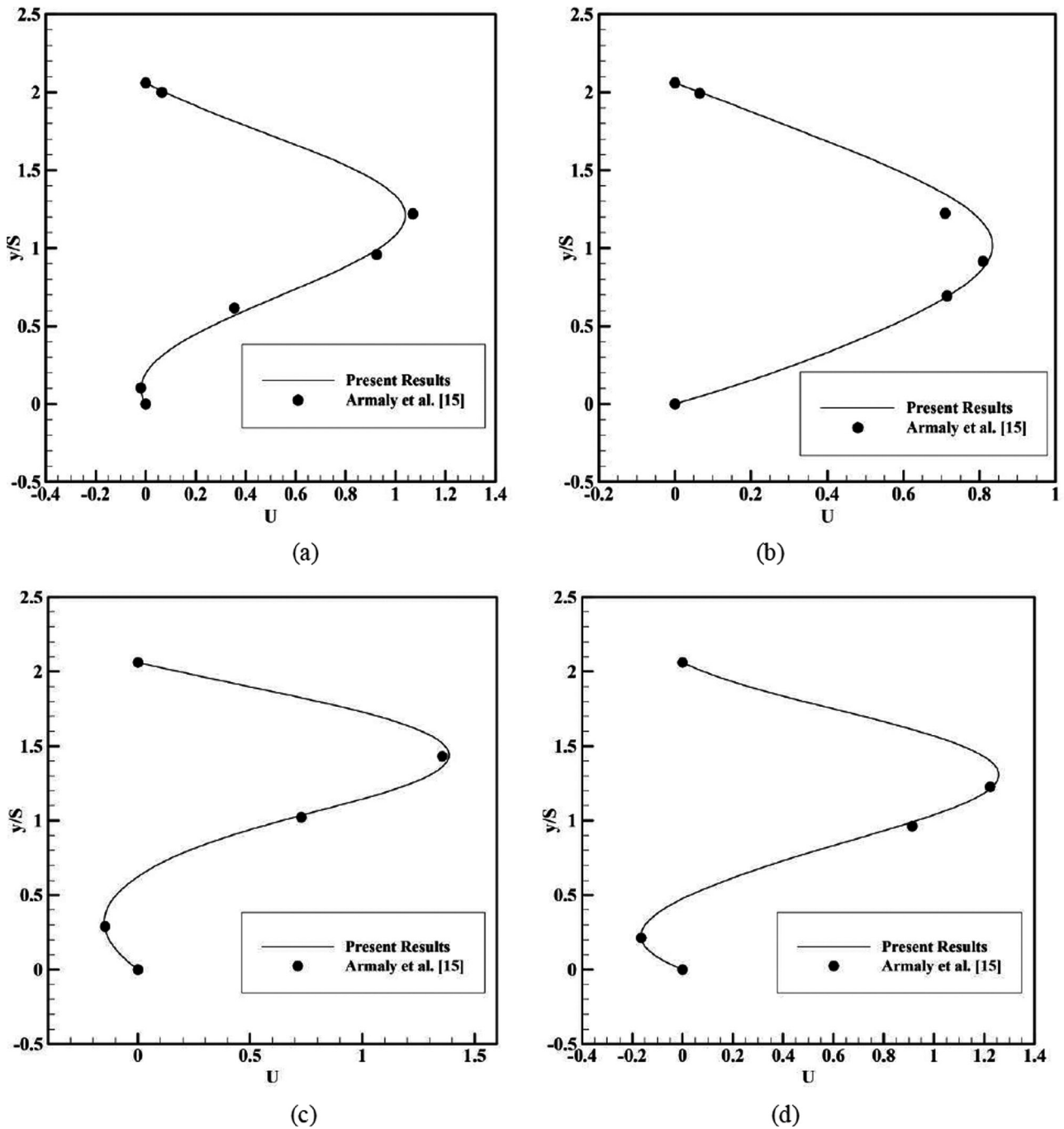|	Armaly et al. [15]		Present results (x/S)	Difference in %	
Re	Experimental x/S	Theoretical x/S		Experimental	Theoretical
100	2.98	2.98	2.96	0.6711	0.6711
389	8.25	7.83	8.08	2.06	3.2

Figure 4. Comparison of the velocity distributions with the results of Armaly et al. [15]. (a) Re = 100 at x/S = 2.55, (b) Re = 100 at x/S = 4.8, (c) Re = 389 at x/S = 2.55 and (d) Re = 389 at x/S = 4.8.

profiles of local Nusselt number along the heated section at Re = 100 - 389 with ϕ = 5%, H_b = 640 μm and D = 1. The figure indicates that the local Nusselt number increases with the rise in Reynolds number. With the increase in Re, the mean velocity increases, improving the mixing phenomena and thus, the heat transfer.

Effect of Baffle Height
Flow structures

The effects of baffle height on hydrodynamic characteristics have been investigated. Four different geometrical configurations have been developed by changing the height of the baffle i.e. H_b = 160 – 640 μm mounted
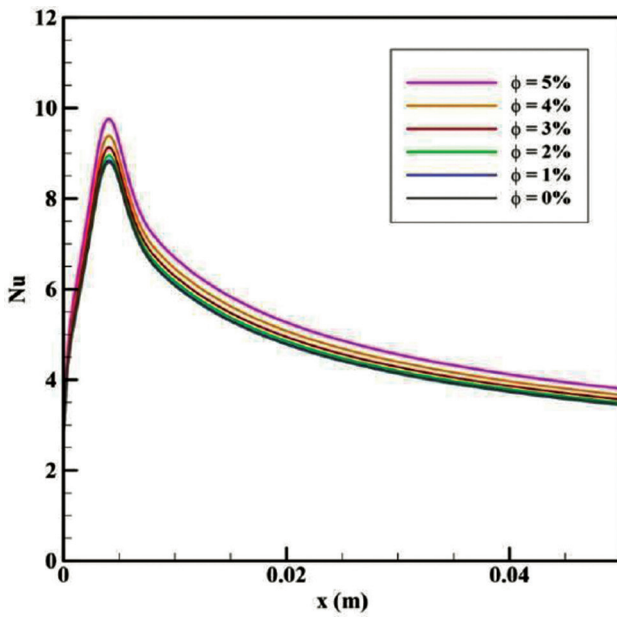
Figure 5. Distribution of local Nusselt along the heated wall at Re = 389 with ϕ = 0 – 5%.

(a)

(b)

Figure 6. Effects of Reynolds number. (a) skin friction coefficient and (b) Nusselt number along the heated wall at Re = 100 – 389 with ϕ = 5%, H_b = 640 μm and D = 1.

at a fixed position of D = 1. Figures 7 (a-e) depict the flow structures at Re = 389 with ϕ = 5%. In the absence of baffle, a primary recirculation zone is formed behind the step due to negative pressure gradient arising due to sudden expansion as shown in Figure 7 (a). The reattachment of the main flow occurs at x/S = 8.08. Additionally, a secondary recirculation zone of small size and strength is also present close to the lower corner between the step and the heated wall. With the insertion of baffle, the flow dynamics is significantly altered as shown in Figures 7 (b-e). A drastic change in the flow structures even with a short baffle of H_b = 160 μm is observed as shown in Figure 7 (b). The main flow is directed towards the lower section of the channel, forming a densely packed region due to contraction caused by the baffle. It can be noticed that there is a reduction in the size of the primary recirculation zone near the step. This causes shifting of the reattachment point of the main flow towards the step direction.

Meanwhile, on the upper section of the channel near the baffle, the appearance of the second secondary recirculation zone consisting of counter-clockwise vortices takes place. When the baffle is elongated to H_b = 320 μm as shown in Figure 7 (c), a peculiar development in the flow structures occurs inside the channel. There is a re-separation of the flow on the heated wall, creating a new secondary recirculation zone in the channel. Also, the primary recirculation zone near the step gets further reduced in size. With further extension of the baffle up to H_b = 640 μm, the primary recirculation region significantly shrinks in size,
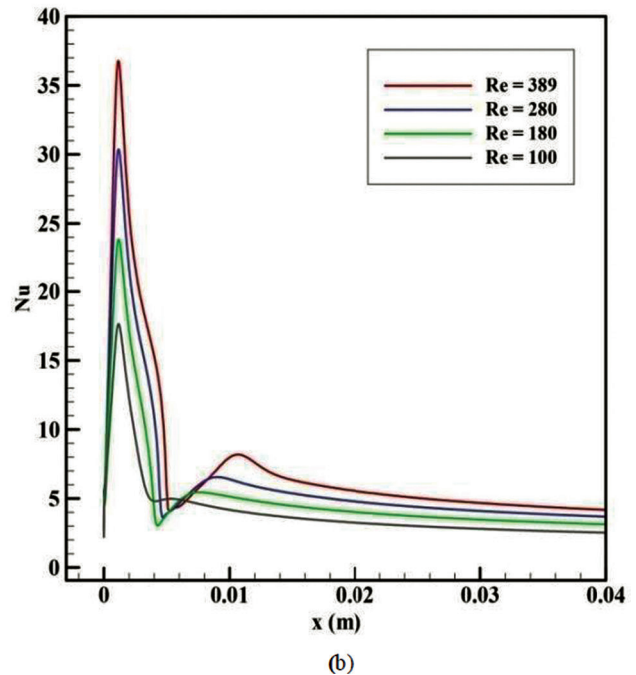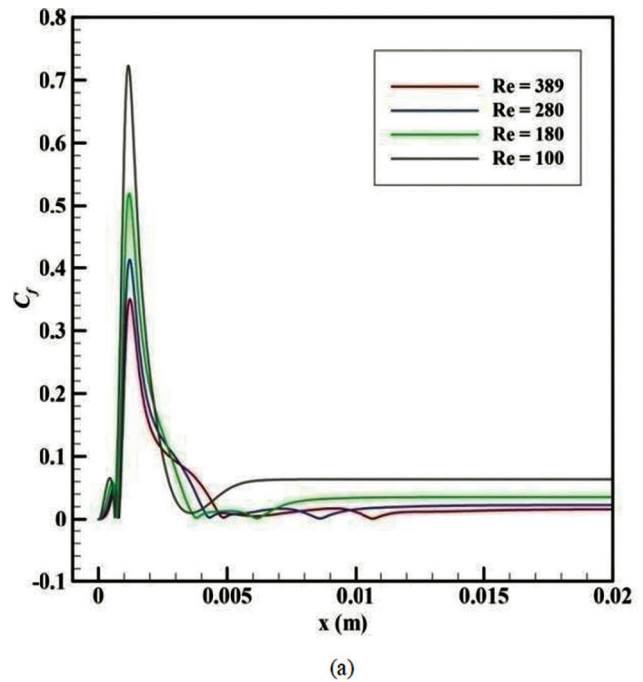
while the secondary recirculation regions on the upper and lower walls grow in size and strength as depicted in Figures 7 (d-e). Figure 8 provides a clear description of the developed flow structures showing multiple recirculation zones formed at different locations in the flow at Re = 389 with ϕ = 5% and D = 1.

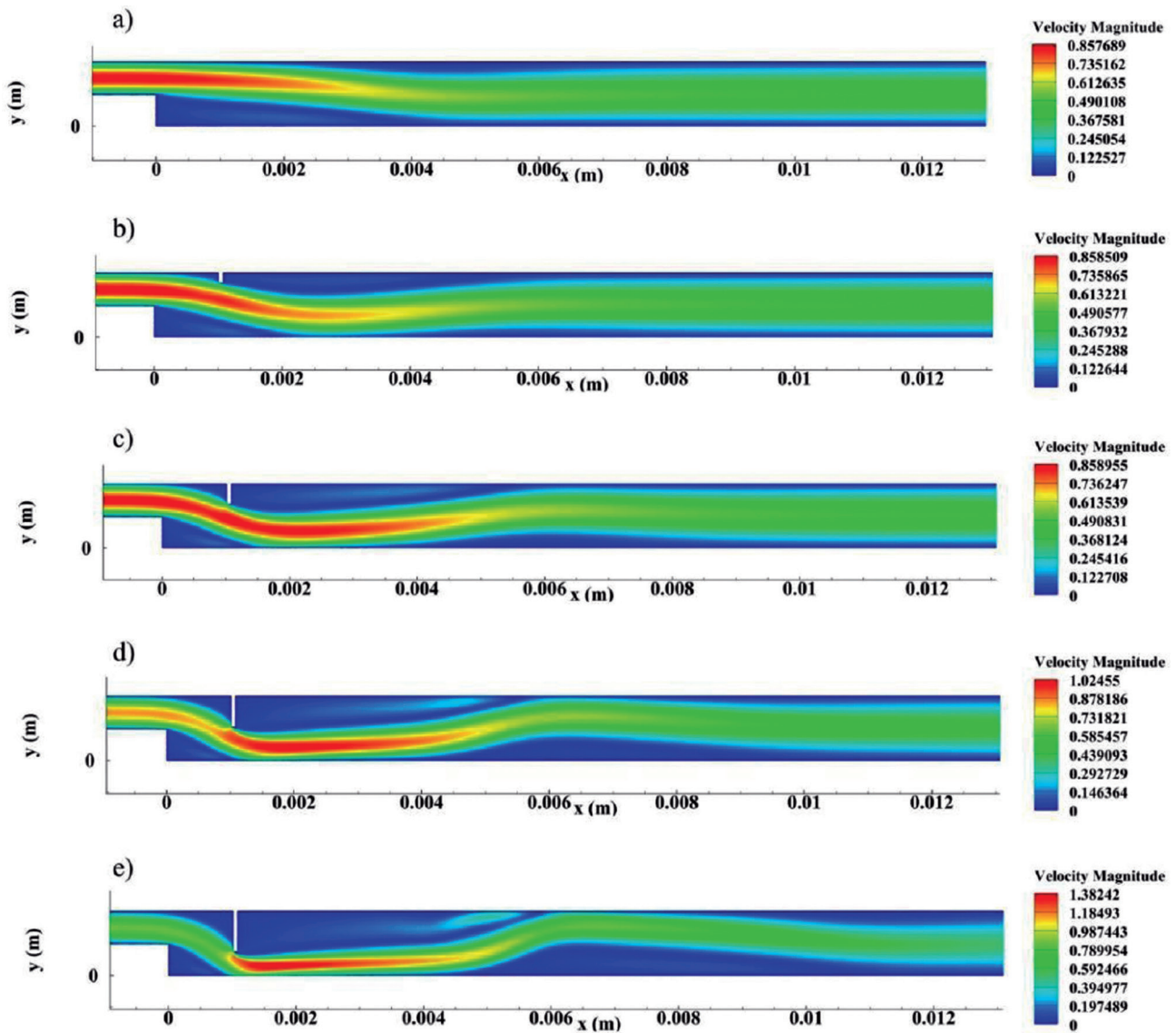**Figure 7.** Effect of baffle height on velocity distribution. (a) no baffle, (b) H_b = 160 μm, (c) H_b = 320 μm, (d) H_b = 480 μm and (e) H_b = 640 μm at Re = 389 with ϕ = 5%.
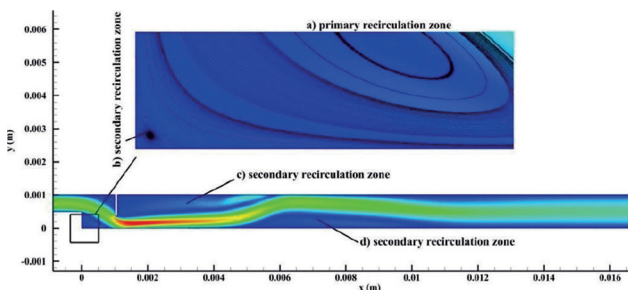

Figure 8. Flow structures. (a) primary recirculation zone near the step, (b) secondary recirculation zone near step corner, (c) secondary recirculation zone at the upper wall and (d) secondary recirculation zone downstream of the lower wall.

Nusselt number

The effect of increasing baffle height from H_b = 160 μm to 640 μm on thermal characteristics has been investigated at Re = 389 with ϕ = 5 and D = 1. Figure 9 (a) shows the distribution of local Nusselt number along the heated wall for the cases with no baffle and aforementioned baffle heights. In the case without baffle, the Nusselt number steeply rises, and reaches the maximum peak near the reattachment point of the primary recirculation region behind the step. Then it slowly decreases downstream of the heated wall due to the thickening of thermal boundary layer and almost a fixed shape is attained. With the addition of baffle, the distribution of Nusselt number is strongly affected. When a short baffle with H_b = 160 μm is installed, the local Nusselt number increases and its peak value is enhanced by about 1.6
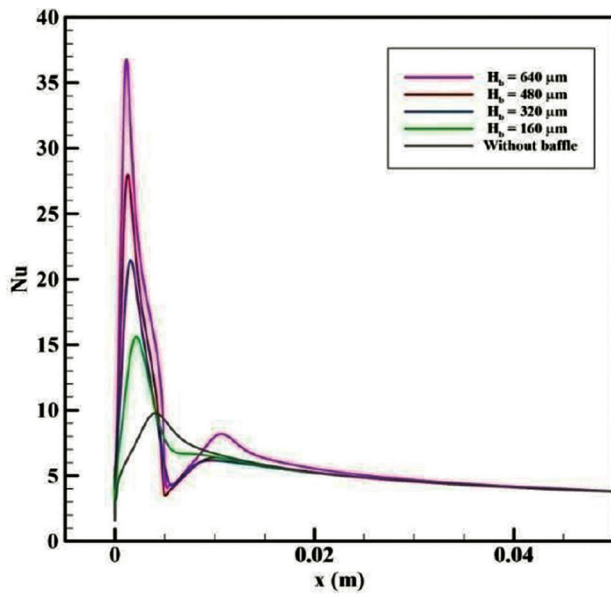
(a)
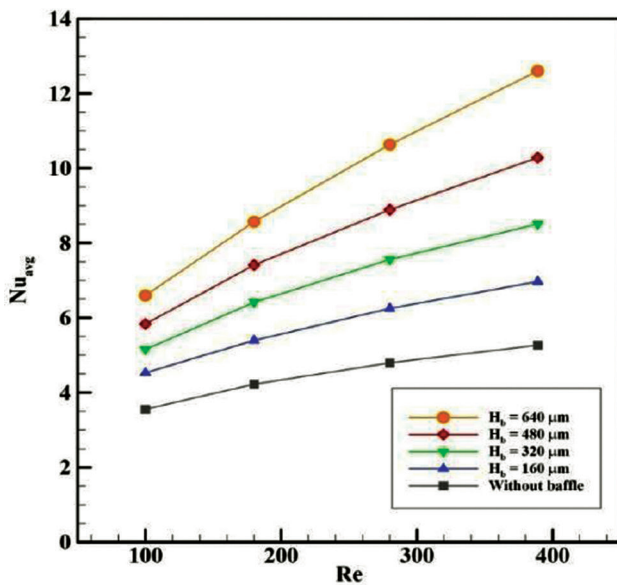
(b)

Figure 9. Effect of baffle height. (a) local Nusselt number at Re = 389 and (b) average Nusselt number at Re = 100 – 389 with ϕ = 5%, H_b = 160-640 μm and D = 1.
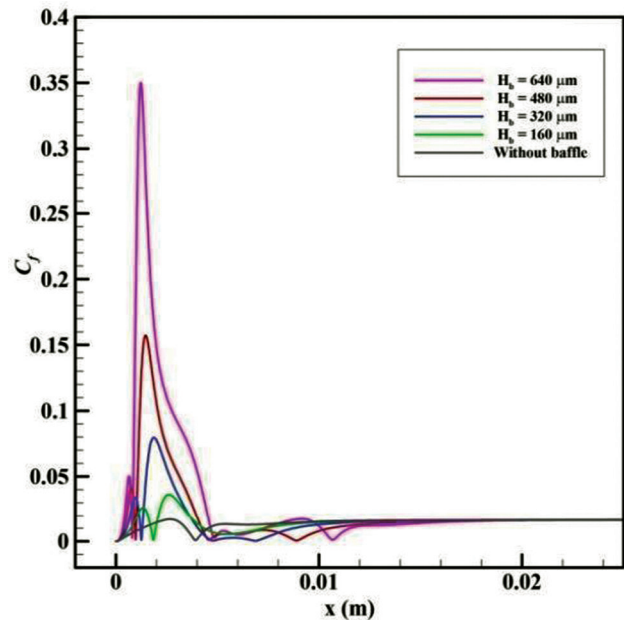

Figure 10. Distribution of local skin friction coefficient along the heated wall for Re = 389 with increasing baffle height.

of local Nusselt number appears at the reattachment point of the secondary recirculation zone formed downstream of the lower wall. The growth in size and strength of the secondary recirculation zone helps the mixing process, thereby enhancing the heat transfer. Results indicate that for baffle heights in the range of H_b = 160 – 480 μm, the location of their maximum peak valuesof Nusselt number is observed outside and slightly away from the compressed primary recirculation zone. For the longest baffle with H_b = 640 μm, the highest value of local Nusselt number occurs slightly away from the baffle side wall after the flow leaves the contracted primary recirculation zone. Figure 9 (b) shows the variation of average Nusselt number at Re = 100 – 389 for the cases with and without baffle. It is clear that the average Nusselt number increases with Reynolds number for all baffle heights, with the maximum value attained at Re = 389 and H_b = 640 μm. Calculations show that the average Nusselt number increased by 164% as compared to the case without baffle.

Skin friction coefficient

The effect of baffle height on skin friction coefficient has been studied. Figure 10 shows the trend of local skin friction coefficient at Re = 389 with ϕ = 5% in the presence of a baffle stationed at D = 1 with increasing heights i.e. H_b = 160 – 640 μm. It is seen that the behavior of local skin friction coefficient is significantly affected with the addition of baffle. In the case of a short baffle with H_b = 160 μm, two peaks of local skin friction coefficient appear due to

times the maximum peak Nusselt number for the case without baffle. This is because the presence of baffle leads to the increase in temperature gradient arising due to the thinning of thermal boundary layer [17]. With a further increase in baffle height, the local Nusselt number drastically increases. When the baffle is elongated from H_b = 160 μm to 640 μm, the peak Nusselt number significantly increases by about 2.4 times the case with H_b = 160 μm. On the other hand, for the case with H_b = 640 μm, a noticeable second peak
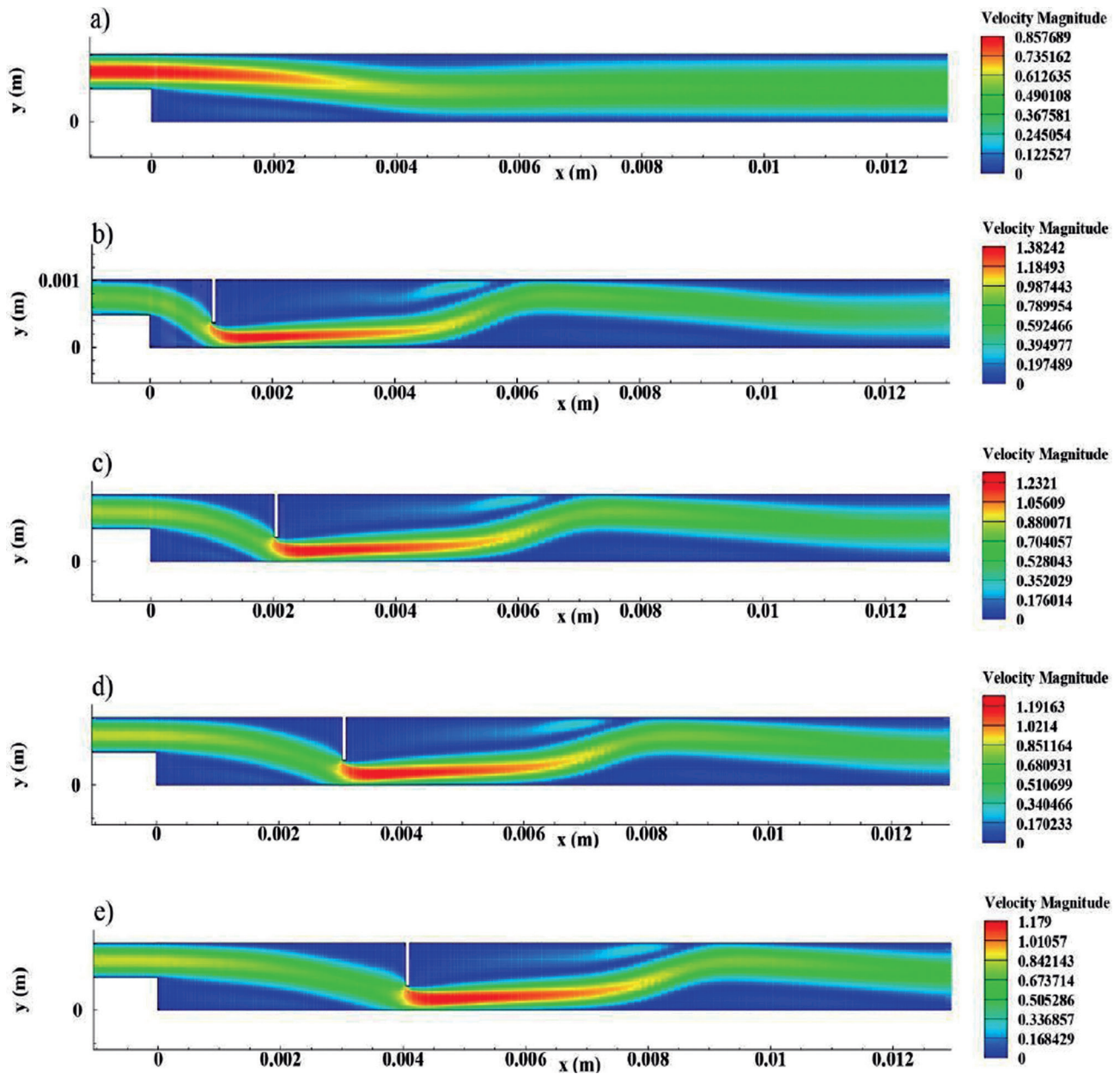
Figure 11. Contours of velocity. (a) no baffle, (b) D = 1, (c) D = 2, (d) D = 3 and (e) D = 4.

the effect of baffle. The minimum peak of local skin friction coefficient corresponds to the compressed primary recirculation zone while the maximum peak is observed outside and slightly away from the compressed primary recirculation zone. With a gradual increase in the baffle height from 160 μm to 640 μm, it can be noticed that the two peaks of the skin friction coefficient rise and is shifted towards the step direction. The rise in skin friction coefficient can be attributed to the fact that the velocity gradient in the flow substantially increases with the increase in baffle height.

For the longest baffle with H_b = 640 μm, the maximum peak value of local skin friction coefficient is seen and is located near the baffle side wall after the flow exits the compressed primary recirculation region.

Effect of Baffle Distance
Flow structures

In this section, the influence of baffle distance on flow structures has been investigated for different baffle positions i.e. D = 1, 2, 3 and 4 on the upper wall of the channel. To
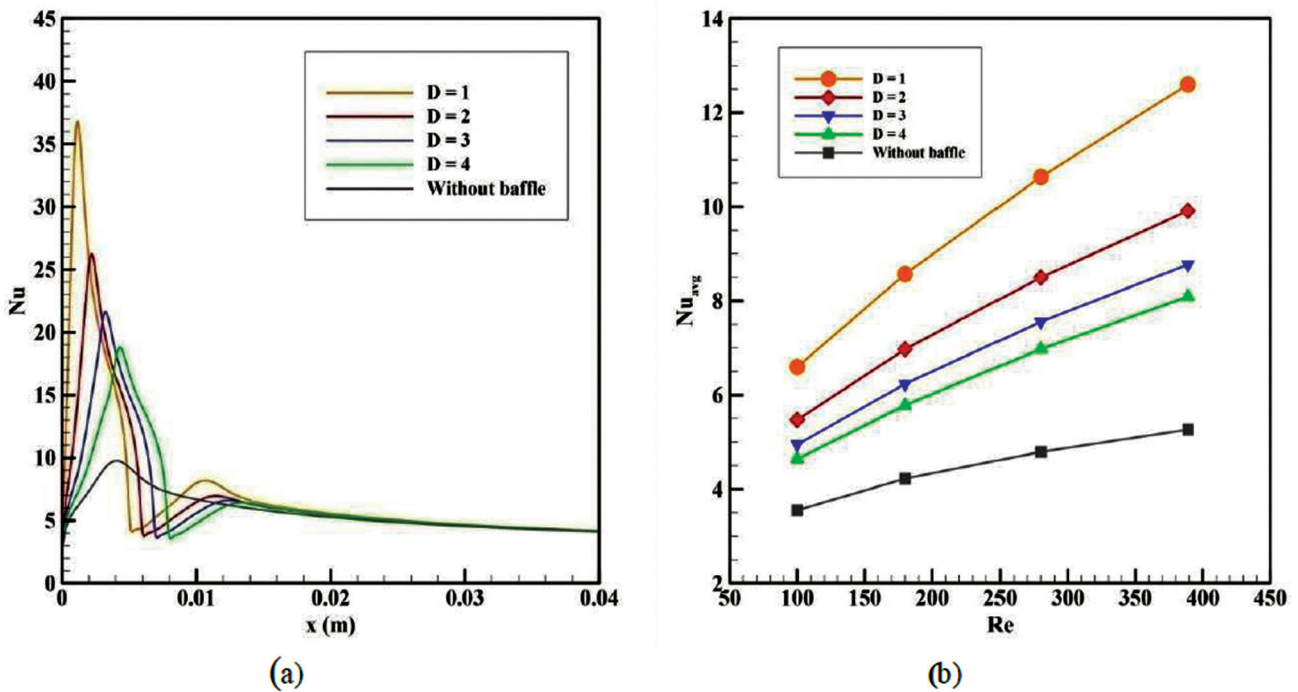
Figure 12. Effect of baffle distance. (a) local Nusselt number at Re = 389, ϕ = 5%, H_b = 640 μm and (b) average Nusselt number at Re = 100 - 389, ϕ = 5% and H_b = 640 μm.

investigate the flow structures inside the channel, the baffle with a fixed height of H_b = 640 μm is moved away from the step i.e. with the increase in D. Results are presented at Re = 389 with ϕ = 5% for geometrical configurations mentioned above as shown in Figures 11(a-e). Figure 11(a) shows the regular flow structure for the case without baffle. When the baffle is located at D = 1, there is the formation of the three recirculation zones at different channel locations as shown earlier in Figure 8. With a gradual movement of the baffle from D = 1 to 4, it can be observed that the size of the primary recirculation zone near the step increases while the secondary recirculation zones at the upper and lower walls shrink in size. Such flow behavior continues to occur when the baffle is placed further away from the step i.e. D = 2 to 4.

Nusselt number

Figure 12 demonstrates the effect of baffle distance (D = 1, 2, 3 and 4) on local Nusselt number along the heated wall at Re = 389 with ϕ = 5% and a fixed height of H_b = 640 μm. Figure 12(a) clearly shows that there is a gradual decrease in local Nusselt number with movement of the baffle away from the step. For all baffle positions, the maximum peak of Nusselt number is attained slightly away from the baffle side wall. Figure 12(b) presents the variation of average Nusselt number with increasing Reynolds numbers for different baffle positions. Results indicate that when the baffle is placed at D = 1, the highest value of average Nusselt number is attained as reported earlier.
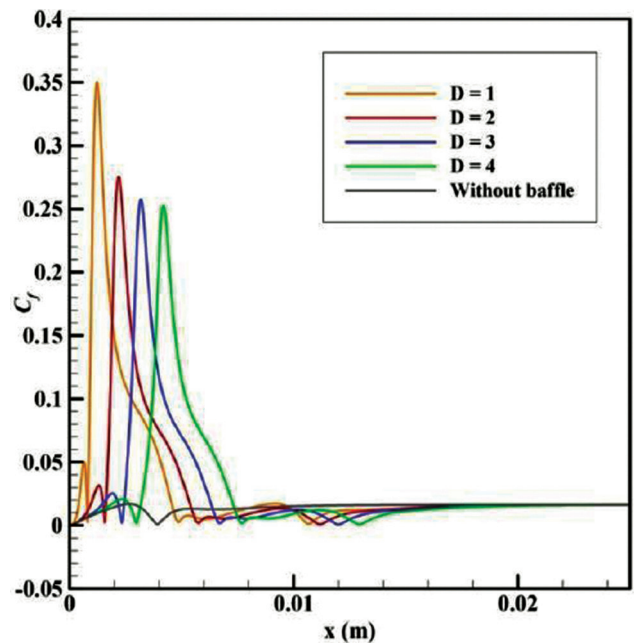

Figure 13. Effect of baffle distance on local skin friction coefficient at Re = 389, ϕ = 5% and H_b = 640 μm.

Skin friction coefficient

The distribution of local skin friction coefficient with increasing baffle distance i.e. D = 1, 2, 3 and 4 at Re = 389

with ϕ = 5% and a fixed height of H_b = 640 μm is shown in Figure 13. It is observed that when the baffle is gradually displaced away from the step, there is decrement in the peak local skin friction coefficient which is located slightly away from the baffle side wall. The maximum peak of local skin friction coefficient is obtained when the baffle is placed at D = 1 and the average skin friction coefficient increased by about 291% as compared to the case without baffle.

CONCLUSION

Numerical investigations were carried out to study the flow and thermal characteristics using water- basedCuO nanofluid at different Reynolds numbers and volume fractions in a micro-scale backward facing step (MBFS) channel with and without baffle. Different geometrical configurations of the MBFS channel were created by changing the baffle height and distance on the upper wall to study their effects on parameters such as velocity distribution, Nusselt number and skin friction coefficient. The conclusions of the present study are as follows:

- The increase in volume fraction and Reynolds number leads to the enhancement of Nusselt number. But the skin friction coefficient decreases with the rise in Reynolds number.
- The analysis of the effects of baffle height and location suggests that there exists an optimum position and height of the baffle under certain flow conditions at which the heat transfer is drastically improved.
- The baffle height has a significant influence on flow and heat transfer. As the baffle is elongated, the Nusselt number is gradually enhanced. Also, the elongation of the baffle causes the primary recirculation zone formed behind the step to decrease, while the secondary recirculation region behind the baffle tends to increase in size.
- The position of the baffle also presents dramatic effects on thermal-hydraulic characteristics. With the increase in the distance between the baffle and the step, the Nusselt number tends to decrease, while the primary recirculation region increases in size.
- The heat transfer increased by 164% when the baffle of height of 640 μm is placed near the step. But the average skin friction coefficient showed increment by 291% as compared to case without baffle. This suggests that an improvement in heat transfer has been achieved with the penalty of increased pumping power requirements.

NOMENCLATURE

H_b	Baffle height, m
d_p	Nanoparticle diameter, m
d_f	Diameter of the base fluid molecule, m
Re	Reynolds number
ER	Expansion ratio
S	Step height, m
D	Dimensionless baffle distance
q_s''	Constant heat flux, W/m^2
d	Baffle distance, m
H	Maximum channel height, m
L_1	Upstream length, m
L_2	Downstream length, m
u	X-velocity, m/s
v	Y-velocity, m/s
v	Kinematic viscosity
U_∞	Freestream velocity
D_h	Hydraulic diameter, m
Nu	Nusselt number
h	Heat transfer coefficient, W/m^{2}K
k	Thermal conductivity, W/mK
C_f	Skin friction coefficient
τ_w	Wall shear stress, Pa
M	Molecular weight of the basefluid, kg
N	Avogadro number
ρ_{f_0}	Mass density of base fluid at reference temperature, kg/m^3
T_0,	Reference temperature, K
C_p	Heat capacity, J/kgK
T	Temperature, K
C_{favg}	Average skin friction coefficient
Nu_{avg}	Average Nusselt number
U	Dimensionless x-velocity
x	Horizontal coordinate, m
y	Vertical coordinate, m

Greek symbols

ϕ	Volume fraction
μ	Dynamic viscosity, kg/ms
α	Thermal diffusivity, m^2/s
ρ	Density, kg/m^3

Subscripts

f	Refers to fluid
p	Refers to nanoparticle

AUTHORSHIP CONTRIBUTIONS

Conceptualization, Shailendra R; methodology, Shailendra R; software, Shailendra R; validation, Shailendra R; formal analysis, Shailendra R; resources, Shailendra R; data curation, Shailendra R; writing- original draft preparation, Shailendra R; writing- review and editing, Shailendra R, Hari BD, Sudip B and Rajendra S; supervision, Hari BD, Sudip B and Rajendra S.

DATA AVAILABILITY STATEMENT

The authors confirm that the data that supports the findings of this study are available within the article.

Raw data that support the finding of this study are available from the corresponding author, upon reasonable request**.**

CONFLICT OF INTEREST

The author declared no potential conflicts of interest with respect to the research, authorship, and/or publication of this article.

ETHICS

There are no ethical issues with the publication of this manuscript.

REFERENCES

[1] Chen Y, Nie T, Armaly BF, Hsieh HT. Turbulent separated convection flow adjacent to backward- facing step—effects of step height. Int J Heat Mass Transf 2006;49:3670–3680. [CrossRef]

[2] Yu W, France DM, Routbort JL, Choi SU. Review and comparison of nanofluid thermal conductivity and heat transfer enhancements. Heat Transf Eng 2008;29:432–460. [CrossRef]

[3] Guo Z. A review on heat transfer enhancement with nanofluids. J Enhanc Heat Transf 2020;27:1–70. [CrossRef]

[4] Abu-Nada E. Application of nanofluids for heat transfer enhancement of separated flows encountered in a backward facing step. Int J Heat Fluid Flow 2008;29:242–249. [CrossRef]

[5] Kherbeet AS, Mohammed HA, Salman BH. The effect of nanofluids flow on mixed convection heat transfer over microscale backward-facing step. Int J Heat Mass Transf 2012;55:5870–5881.

[6] Ekiciler R. A CFD investigation of Al_2O_3/water flow in a duct having backward-facing step. J Therm Eng 2019;5:31–41. [CrossRef]

[7] Abdulvahitoglu A. Using analytic hierarchy process for evaluating different types of nanofluids for engine cooling systems. Therm Sci 2019;23:3199–3208. [CrossRef]

[8] Kilic M, Abdulvahitoglu A. Numerical investigation of heat transfer at a rectangular channel with combined effect of nanofluids and swirling jets in a vehicle radiator. Therm Sci 2019;23:3627–3637. [CrossRef]

[9] Heshmati A, Mohammed HA, Parsazadeh M, Fathinia F, Wahid MA, Sies MM, et al. Effect of vertical baffle installation on forced convective heat transfer in channel having a backward facing step. Appl Mech Mater 2013;388:169–175. [CrossRef]

[10] Alawi OA, Che Sidik NA, Mohammed HA. Assisted and opposed mixed convective nanofluids flow over vertical backward facing step having a baffle. J Comput Theor Nanosci 2015;12:2048–2061. [CrossRef]

[11] Abuldrazzaq T, Togun H, Alsulami H, Goodarzi M, Safaei MR. Heat transfer improvement in a double backward-facing expanding channel using different working fluids. Symmetry 2020;12:1088. [CrossRef]

[12] Khanafer K, Vafai K, Lightstone M. Buoyancy-driven heat transfer enhancement in a two-dimensional enclosure utilizing nanofluids. Int J Heat Mass Transf 2003;46:3639–3653. [CrossRef]

[13] Corcione M. Heat transfer features of buoyancy-driven nanofluids inside rectangular enclosures differentially heated at the sidewalls. Int J Therm Sci 2010;49:1536–1546. [CrossRef]

[14] Xuan Y, Li Q. Investigation on convective heat transfer and flow features of nanofluids. J Heat Transf 2003;125:151–155. [CrossRef]

[15] Armaly B, Durst F, Pereira J, Schönung B. Experimental and theoretical investigation of backward-facing step flow. J Fluid Mech 1983;127:473–496. [CrossRef]

[16] Kumar, S, Prasad, SK., Banerjee, J. Analysis of flow and thermal field in nanofluid using a single phase thermal dispersion model. Appl Math Model 2010;34:573–92. [CrossRef]

[17] Ma, Y, Mohebbi, R, Rashidi, MM, Yang, Z, Fang, Y. Baffle and geometry effects on nanofluid forced convection over forward-and backward-facing steps channel by means of lattice Boltzmann method. Phys A: Stat Mech Appl 2020;554:124696. [CrossRef]